

# DOWNSTREAM EVOLUTION OF A LAMINAR SPOT

**Akira MATSUMOTO**

**College of Science and Technology, Nihon University,  
1-8 Kanda Surugadai Chiyoda-Ku, Tokyo 101- 8308, Japan**

**Keywords:** *Boundary layer transition, Hot wire anemometer, Turbulent spot*

## **Abstract**

*It was well known that the disturbance, introduced artificially into a supercritical two-dimensional laminar boundary layer along a flat plate by ejecting an intermittent jet from a small hole on the flat plate, developed downstream and finally evolved into a turbulent spot. As a jet and the Reynolds number match well, however, this disturbance was still laminar during the initial stage of its downstream evolution and resembled a turbulent spot. Therefore, we called it a 'laminar spot'. We focused our attention on the transition of a laminar spot to a turbulent spot. Measurements were made of streamwise mean velocity and turbulence intensity profiles of a laminar boundary layer in detail using the multi-channel data processing connected with the rake type 16-channel hot-wire anemometer system. Moreover, we visualized the flow field with a laminar spot by drawing several contours of difference between streamwise mean velocity and Blasius velocity. As a result, we found that a laminar spot consists of high-speed and low-speed regions lined up alternately in spanwise direction. At the first stage of its downstream evolution, a laminar spot grows slowly to spanwise direction. The half of lateral growth can be estimated as 5°, which was almost half of a turbulent spot growth. At the next stage, lateral growth of a laminar spot is repressed. After then, it is traveling downstream with the same growth angle, about 10°, as that of a turbulent spot. Thus, we deduce that this stage might be the beginning of transition from a laminar to a turbulent spot.*

## **1 Introduction**

There are many researchers who have studied a transition from laminar to turbulent boundary layer. Emmons [1] observed carefully that there occurred suddenly small turbulent sources, irregular in shape, in natural transition of the critical Reynolds number and it spread out downstream in all directions, finally grew up into turbulent spots. As a result, he assumed (1) point-like breakdown, (2) a sharp boundary between the turbulent fluid of a spot and the surrounding laminar flow, (3) a uniform rate of spot growth and (4) no interaction between spots. Schubauer and Klebanoff [2] confirmed Emmons' assumptions except for (4) experimentally in detail. They introduced a turbulent spot artificially into a laminar boundary layer on the flat plate by the electric spark, because it did not reappear at same station in natural transition, so it was difficult to catch it by the hot-wire probe. Elder [3] gave experimental evidence for Emmons' fourth assumption that the area of a flat plate covered with turbulent fluid was simply the combined area of the turbulent spots presented assuming each spot grew independently of all the others. However, we do not agree with this evidence.[4] Coles and Barker [5] also pointed out that the periodic fluctuation remained downstream into turbulent boundary layer tripped by the row of strong point-disturbances for a long distance. Amini and Lespinard [6] investigated experimentally a laminar disturbance, an incipient spot, prior to a turbulent spot in a subcritical transitional boundary layer. Moreover, Komoda et al. [7] have found such a

spot even in supercritical boundary layer and examined its downstream development.

The purposes of the present study are: ① to examine in more detail how a laminar spot develops downstream; and ② to clarify the transition from a laminar to a turbulent spot.

## 2 Experimental Apparatus and Procedures

Experiments were performed in a low speed wind tunnel. This wind tunnel was a closed return-circuit type and contained a test section  $1\text{ m} \times 0.4\text{ m} \times 3.1\text{ m}$  in size. Measurements were made of instantaneous streamwise velocity and turbulence intensity profiles of the laminar boundary layer perturbed by small jet along the flat plate  $2.5\text{ m}$  long,  $1\text{ m}$  wide bakelite plate, mounted vertically in the test section. The small hole of  $1\text{ mm}$  in diameter was drilled on the surface of the flat plate at  $75\text{ cm}$  downstream from the leading edge as shown in Fig.1 (a). A jet ejected from the hole by a loudspeaker at  $250\text{ ms}$  intervals gave an initial-disturbance to the supercritical two-dimensional laminar boundary layer. The instantaneous and fluctuating velocity were measured with a linearized hot-wire anemometer system. The probe used contained 16 hot-wires placed at  $2\text{ mm}$  spaces in a row in spanwise direction as shown in Fig.1 (b). As the spot, which was formed whenever the jet generator was triggered, passed through the probe, the streamwise instantaneous velocity of the whole spot was collected using the multi-channel data processing equipment, which consists of the 16-channel 12-bit A/D converters and 4MW/CH acquisition memory, connected with 16-channel hot-wire anemometer system. The internal structure of the spot depends strongly on the Reynolds number and the intensity of the jet. Thus, in order to retain the spot's reproducibility at the same streamwise position, the Reynolds number based on the displacement thickness  $\delta^*$  at the hole and free stream velocity  $U_0$ ,  $Re_{\delta^*} = U_0 \delta^* / v$ , where  $v$  is kinetic viscosity, was kept to 990 and the estimated vertical jet velocity was as large as 0.65 times the free stream velocity. The free stream turbulence intensity was below 0.07 % in

$U_0 = 10\text{ m/s}$ . The streamwise direction is denoted by  $x$ ; the wall-normal direction, by  $y$  and the spanwise direction, by  $z$ , and the origin of the axes is taken at the hole.

## 3 Results and Discussion

### 3.1 Feature of the laminar spot

Figure 2 shows velocity profiles  $U/U_0$  plotted versus  $y/\delta^*$  ( $\delta^*$  being displacement thickness) for undisturbed boundary layer. All plots were in good agreement with the Blasius profile shown as a solid line. Thus, this figure reveals that the boundary layer flow maintained laminar within the limits of this experiment. Then, we ejected a jet as shown in Fig.1 (a) from a small hole and gave some disturbances to the laminar boundary layer for short duration.

Figure 3 and 4 show the typical plan-view and side-view of  $\Delta U_{\text{mean}}/U_0$  contours respectively for a spot. Where  $\Delta U_{\text{mean}}$  represents velocity-deviation,  $U_{\text{mean}} - U_b$ , subtracted the Blasius profile velocity  $U_b$  for the undisturbed boundary layer from the ensemble averaged velocity  $U_{\text{mean}}$ , and  $U_0$  free stream velocity,  $T$  is time since trigger pulse was generated. Figure 3 (a), (b), (c) indicate that, at a typical  $y$ -position,  $y = 1.4\text{ mm}$ , this spot consisted of high-speed ( $\Delta U_{\text{mean}} > 0$ ) and low-speed ( $\Delta U_{\text{mean}} < 0$ ) regions, and they lined up alternately in spanwise direction. Moreover, we can see that high-speed regions appeared outside of low-speed regions at  $z = \pm 5\text{ mm}$ . This indicates that the spot was growing outward as it traveled downstream, because these high-speed regions did not exist at  $x = 40\text{ mm}$  and  $60\text{ mm}$ .

Figure 4(a), (b), (c) show that there were some low-speed protuberances with high-shear layers in line over the high-speed region at  $z = 0$ . It seems that they were the low-speed regions that introduced by the hairpin vortices. The first protuberance was out of the undisturbed laminar boundary layer thickness ( $y \approx 6.5\text{ mm}$ ). Moreover, we can see that there were high-shear layers, becoming unstable and generating hairpin vortices, for example, at  $x = 80\text{ mm}$  and

$y = 4\text{mm}$ , at  $T = 32.5\text{m sec}$ . As a result, the number of the protuberance increased with a spot developing downstream as shown later.

As described previously, the spot was growing outward. Then, we examined the transverse growth of the spot as shown in Fig.5. We defined the outline of the spot as  $|\Delta U_{\text{mean}} / U_0| \geq 0.02$  at  $y = 1.4\text{mm}$ .

From this figure, it is found that, at the first stage to  $x=90\text{mm}$ , the half angle of transverse growth of a spot can be estimated as  $5^\circ$ , which was almost half of turbulent spot growth [8]. At the next stage, from  $x=90\text{mm}$  to  $130\text{mm}$ , transverse growth of a spot was repressed. After then, it was traveling downstream with the same growth angle, about  $10^\circ$ , as that of a turbulent spot. These results reveal that, at the first stage, the spot was not a turbulent spot but an incipient spot. Thus, we named this kind of the spot ‘laminar spot’. Furthermore, we expected ‘plateau’ in Fig.5 as the starting point that the spot indicated the transition from laminar to turbulent state. Figure 6 shows the propagation velocities of the spot. It is found a velocity of  $0.92U_0$  for the front and  $0.47U_0$  for the tail. It is the same velocity as that of a turbulent spot [8] but different from that of a three-dimensional wave packet ( $0.44U_0$  for the front,  $0.36U_0$  for the tail) [6]. This result means that the rate of elongation was basically same both in a laminar spot and in a turbulent spot.

### 3.2 Feature of the transitional spot

As stated previous section, we deduced that the ‘plateau’ in Fig.5 might be the beginning of transition from a laminar to a turbulent spot. In this section, we discuss about the hairpin vortices playing an important role in a turbulent spot. Figure 7 shows the propagation velocities of the low-speed protuberances at  $z=0$ , and at  $z=-5\text{mm}$ . All of them traveled at the constant speed respectively. Especially, both the first and the second protuberance at  $z=0$  were produced immediately after the jet ejected and had almost the same convective speeds ( $\approx 0.9U_0$ ) as that of the front of the spot. On the other hand, the third and the fourth protuberance were newly born at

$x=100\text{mm}$ , and at  $x=130\text{mm}$  respectively. Each one also had the different speeds. Moreover, they were slower than the previous two ( $U_p = 0.8U_0$  for the third protuberance,  $U_p = 0.64U_0$  for the fourth one). Consequently, the hairpin vortices surrounding these low-speed protuberances were strengthened due to its elongation. In addition, the new protuberance with the convective speed  $U_p = 0.6U_0$  was produced at about  $z=-5\text{mm}$ .

Figure 8 shows the front view of contours of the spot. First, the spot grew sharply outward ① and then, it was repressed ② at  $y \approx 1.5\text{mm}$  ( $y/\delta^* \approx 0.59$ ), already shown in Fig.5. However, we can see that the new growth of the spot begun ③ at  $y \approx 3\text{mm}$  ( $y/\delta^* \approx 1.3$ ) when we turned our eyes upward. This is why, at the ‘plateau’, high-shear layer located behind the last protuberance was more strengthened than that in ‘Laminar spot region’ as shown in Fig.9. The hairpin vortex was therefore intensified by the induced velocity due to the streamwise vortices on the centerline and shear-layer in the low-speed region at about  $z=-5\text{mm}$  became stronger. As a result, the ‘low-speed wing’ was born from the low-speed region at about  $z=-5\text{mm}$ , at  $x=110\text{mm}$  and developed rapidly outward with the spot traveling downstream as shown in Fig.10. This ‘low-speed wing’ contributed to the lateral growth of the spot at  $y \approx 3\text{mm}$ .

Figure 11(a), (b), (c) show the downstream development of the outside low-speed region as already shown. At the final stage of the ‘plateau’ ( $x=130\text{mm}$ ), the head of the low-speed region sharpened and high-speed region ran deep into low-speed one. This structure is similar to that of the centerline in shape. Furthermore, normalized velocity gradient ( $\delta^*/U_0)(\partial U/\partial y)$  also became stronger at the back of low-speed region, and at the boundary of high-speed and low-speed regions. As a result, we imagine that the hairpin vortex surrounding low-speed regions was growing.

### 3.3 Turbulence field of the spot

Figure 13 and 14 show the turbulence intensity  $u'/U_0$  at  $z=0$  and  $z=-5\text{mm}$  or  $-6\text{mm}$ ,  $u'$  is the r.m.s value of fluctuating velocity in streamwise direction. Turbulence intensity level was below 3% even at the protuberance with high-shear layer at  $x=100\text{mm}$  as shown in Fig.13 (a). This reveals that the spot was still laminar. In  $x=130\text{mm}$ , the maximum turbulence intensity level was locally at most 5% as shown in Fig.13 (b). Nevertheless, Figure 14(b) shows that turbulent regions spread a little outward. As the spot reached  $x=170\text{mm}$  where it had some resemblance to a turbulent spot, turbulent regions above 1% spread over the whole spot. Figure 13 (c) shows that turbulence was largely generated both by the high-shear layer in the low-speed regions, about 9%, and by the shear-layer in vicinity of the wall surface, about 7%. Furthermore, there is the high-level turbulence (about 10%) generated at the outside of the spot ( $z=-6\text{mm}$ ) as shown in Fig.14(c). In order to understand the lateral spread of turbulent regions of the spot, we examine that the contours of normalized velocity gradient  $(\delta^*/U_0)(\partial U/\partial z)$  as shown in Fig.15 (a), (b), (c). T indicated in the caption means the time when the top of the outside low-speed regions was just passing the hot-wire probes. In  $x=100\text{mm}$ , the remarkable regions of  $\partial U/\partial z > 0$  diagonally expanded upward from the centerline,  $z=0$ . There were some turbulence generations along with these regions as shown in Fig.16 (a). In addition, we can see the regions of  $\partial U/\partial z < 0$  near the outside low-speed regions of the spot. This indicates the growth of hairpin vortex around these regions. As the spot was growing downstream, the regions of  $\partial U/\partial z > 0$  mingled more and more with those of  $\partial U/\partial z < 0$ . For these three-dimensional distortions in the spot, turbulence regions spread outward and those intensity was strengthened as shown in Fig.16 (b), (c).

#### 4 Conclusions

We examine some contours of velocity-deviation and velocity fluctuation in a transitional spot that was artificially produced

into a supercritical two dimensional laminar boundary layer along a flat plate by ejecting intermittent jet from small hole.

Results obtained are summarized as follows,

- (1) At ‘Laminar spot region’, a spot consists of high-speed and low-speed regions line up alternately in spanwise direction and then, the half of lateral growth is estimated as  $5^\circ$ . Moreover, turbulence is less and locally generated yet.
- (2) At the first stage of ‘Transition region’, the transverse growth of the spot is repressed at  $y/\delta^* \approx 0.59$ , nevertheless, the ‘low-speed wing’ is newly born from the outer low-speed regions of the spot and it contributes to the new transverse growth at  $y/\delta^* \approx 1.3$ .
- (3) While this ‘low-speed wing’ emerging, the spot is largely distorted and its structure become complicated more and more. As a result, we deduce that this stage might be the beginning of transition from a laminar to a turbulent spot.

#### References

- [1] Emmons, H.W. The laminar-turbulent transition in a boundary layer. Part I . *J. Aero.Sci.*, Vol.18, pp.490, 1951.
- [2] Schubauer, G.B. and Klebanoff, P.S. Contributions on the mechanics of boundary-layer transition. *NACA Tech. Note*, 3489, 1955.
- [3] Elder, J.W. An experimental investigation of turbulent spots and break down to turbulence. *J.Fluid Mech.*, Vol.9, pp.235, 1960.
- [4] Sugamata, T. and Matsumoto, A. Interaction of disturbances formed artificially by thin jets. *Second Pacific Asia Conference On Mechanical Engineering*, Manila, Philippines, pp409, 1998.
- [5] Coles, D. and Barker, S.J. Some remarks on a synthetic turbulent boundary layer. *Turbulent mixing in nonreactive and reactive flow*, Plenum, pp.285, 1975.
- [6] Amini, J. and Lepinard, G. Experimental study of an ‘incipient spot’ in a transitional boundary layer. *Phys. Fluids*, Vol.25, No.10, pp1743, 1982.
- [7] Komoda, H., Handa, N. and Matsumoto, A. Downstream development of a laminar spot. *J. Japan Soci. Fluid Mech.*, Vol.13, pp.222, 1994.
- [8] Wygnanski, I., Sokolov, M. and Friedman, D. On a turbulent ‘spot’ in a laminar boundary layer. *J. Fluid Mech.*, Vol.78, part4, pp785, 1976.

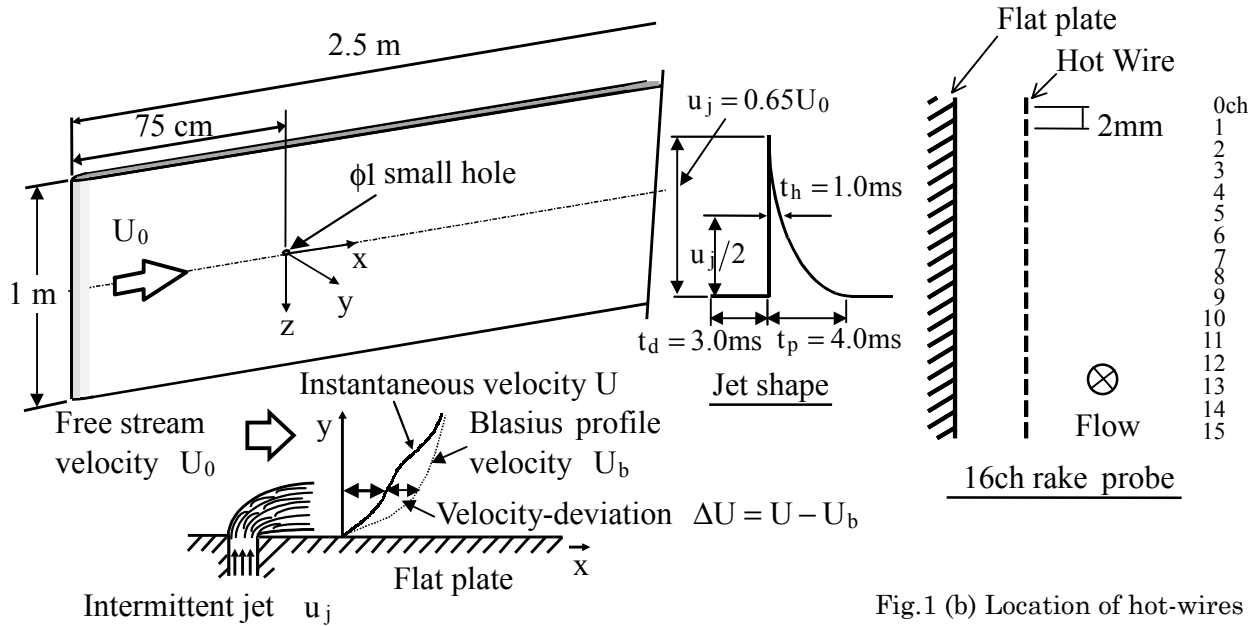


Fig.1 (a) Flat plate and Jet shape

Fig.1 (b) Location of hot-wires

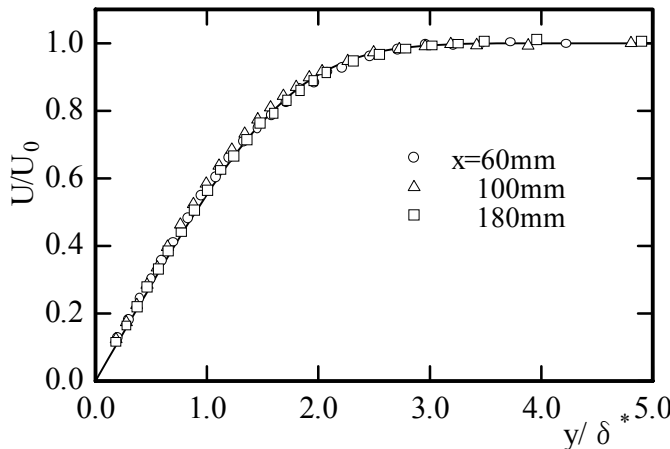


Fig.2 Velocity profiles for the undisturbed boundary layer. All plots are good agreement with Blasius profiles (Solid line).

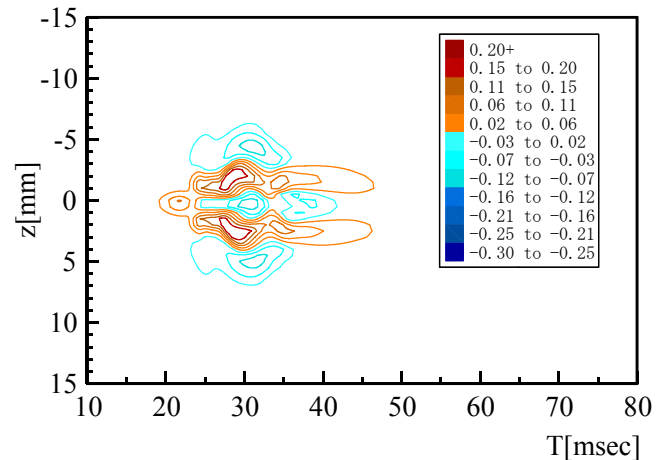


Fig.3 (b) Plan view of  $\Delta U_{\text{mean}}/U_0$  for a laminar spot.  $x = 60\text{mm}$ ,  $y = 1.4\text{mm}$ .

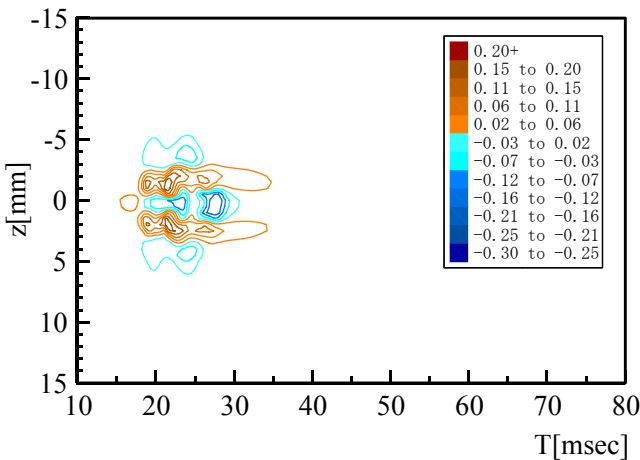


Fig.3 (a) Plan view of  $\Delta U_{\text{mean}}/U_0$  for a laminar spot.  $x = 40\text{mm}$ ,  $y = 1.4\text{mm}$ .

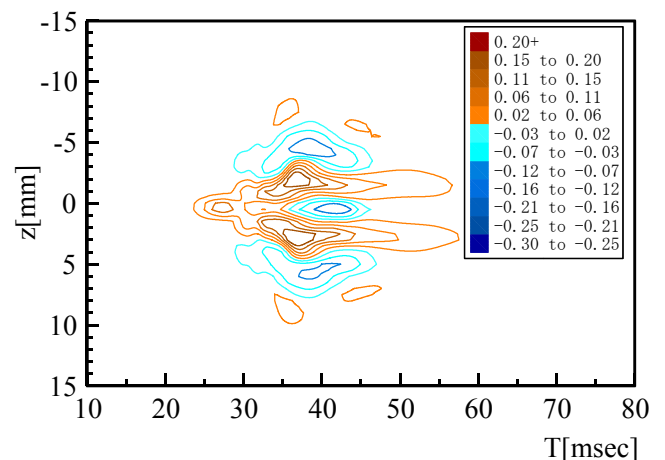


Fig.3 (c) Plan view of  $\Delta U_{\text{mean}}/U_0$  for a laminar spot.  $x = 80\text{mm}$ ,  $y = 1.4\text{mm}$ .

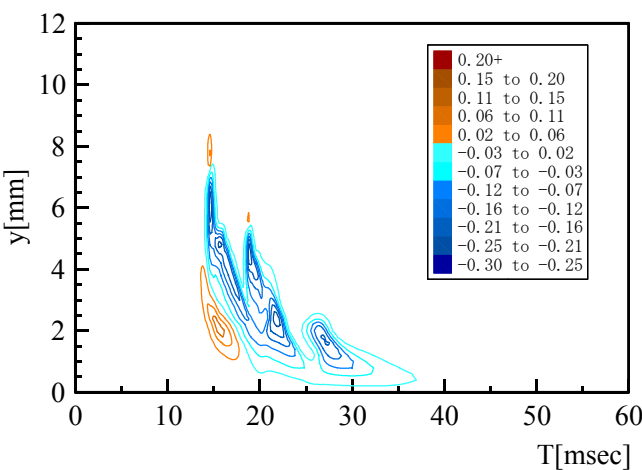


Fig.4 (a) Side view of  $\Delta U_{\text{mean}}/U_0$  contour for a laminar spot.  $x=40\text{mm}$ ,  $z=0$ .

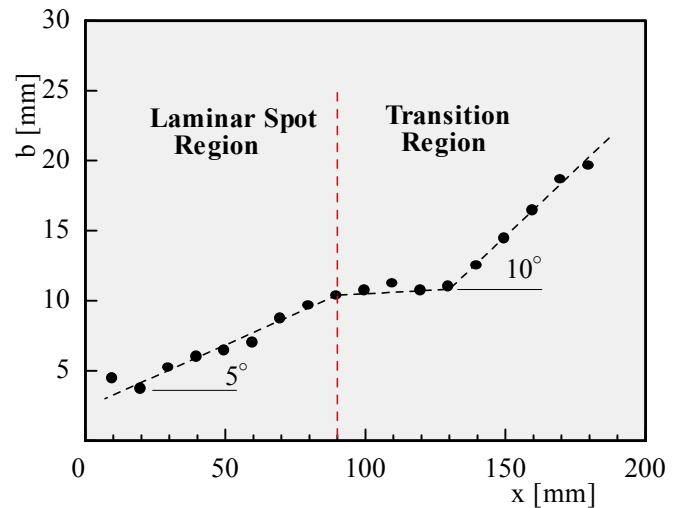


Fig.5 Transverse growth of a spot

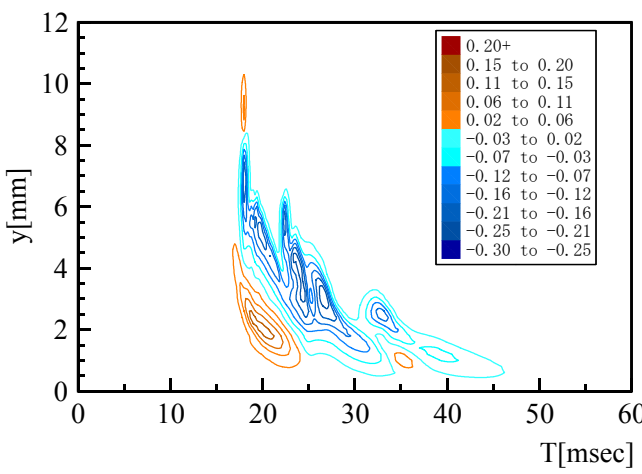


Fig.4 (b) Side view of  $\Delta U_{\text{mean}}/U_0$  contour for a laminar spot.  $x=60\text{mm}$ ,  $z=0$ .

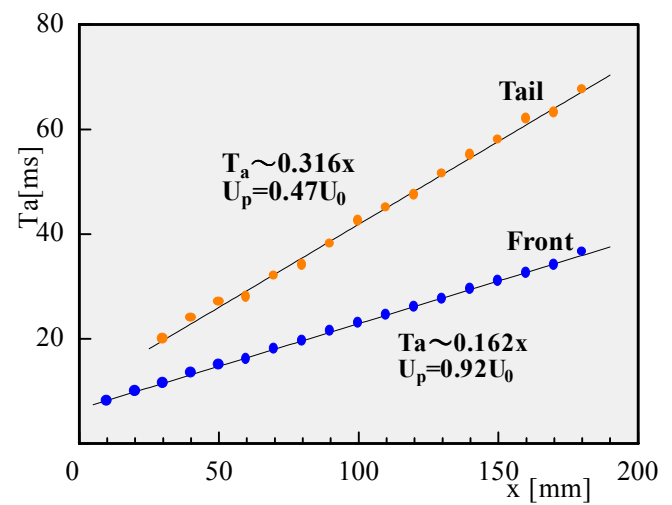


Fig.6 Propagation velocities of a spot

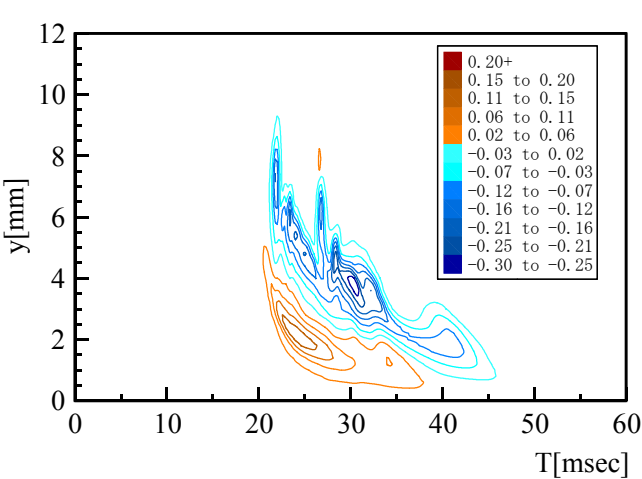


Fig.4 (c) Side view of  $\Delta U_{\text{mean}}/U_0$  contour for a laminar spot.  $x=80\text{mm}$ ,  $z=0$ .

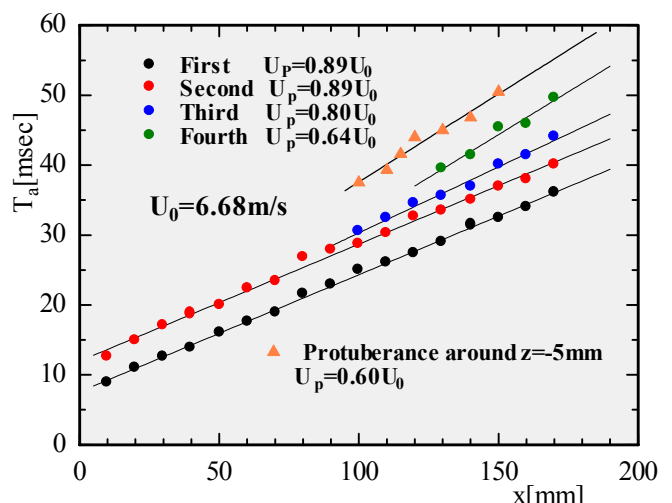


Fig.7 Propagation velocities of the protuberances

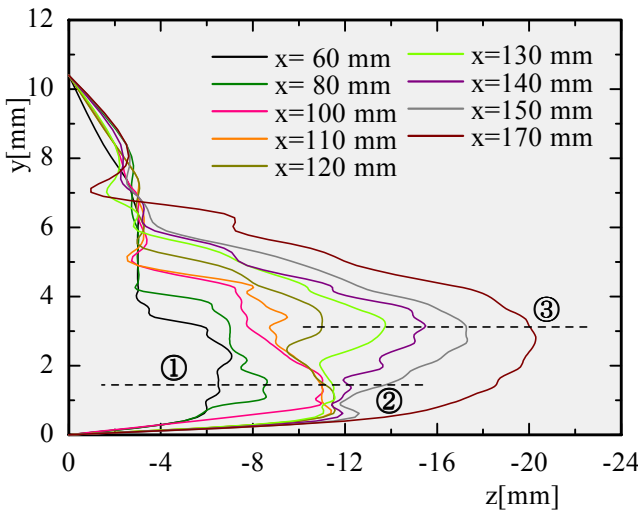


Fig. 8 Contours of the spot

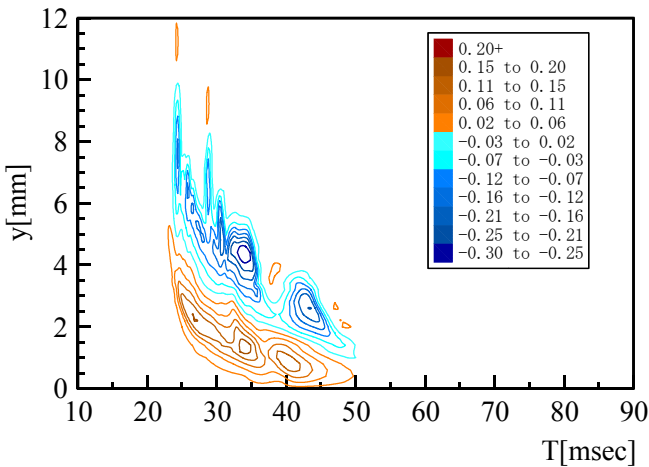


Fig. 9 (a) Side view of  $\Delta U_{\text{mean}}/U_0$  contour  
for a spot in the transition region.  
 $x=100\text{mm}$ ,  $z=0$ .

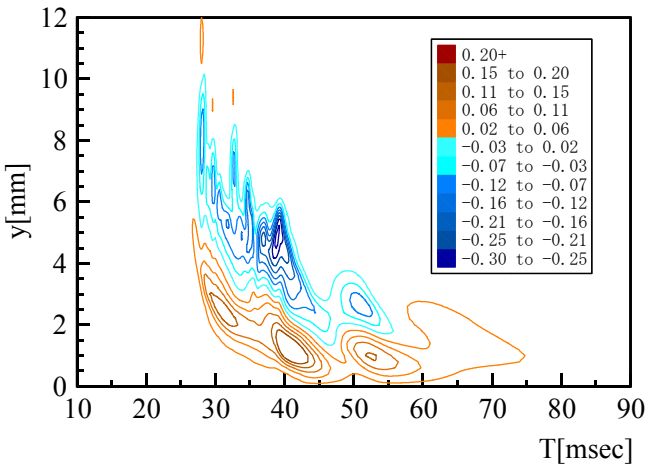


Fig. 9 (b) Side view of  $\Delta U_{\text{mean}}/U_0$  contour  
for a spot in the transition region.  
 $x=120\text{mm}$ ,  $z=0$ .

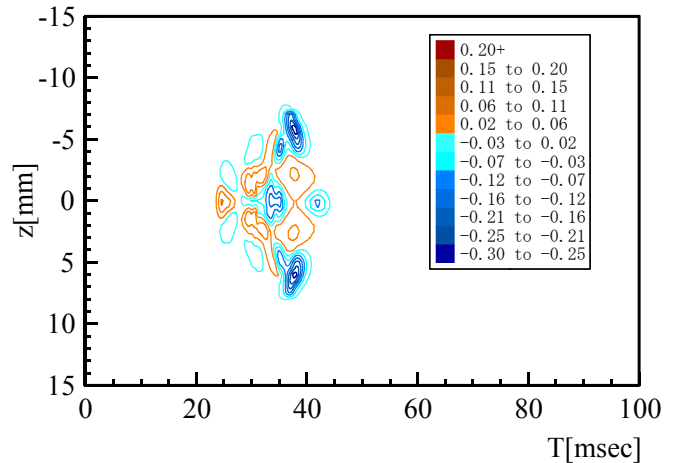


Fig. 10. (a) Plan view of  $\Delta U_{\text{mean}}/U_0$  contour  
for a spot in the transition region.  
 $x=100\text{mm}$ ,  $y=3.4\text{mm}$ .

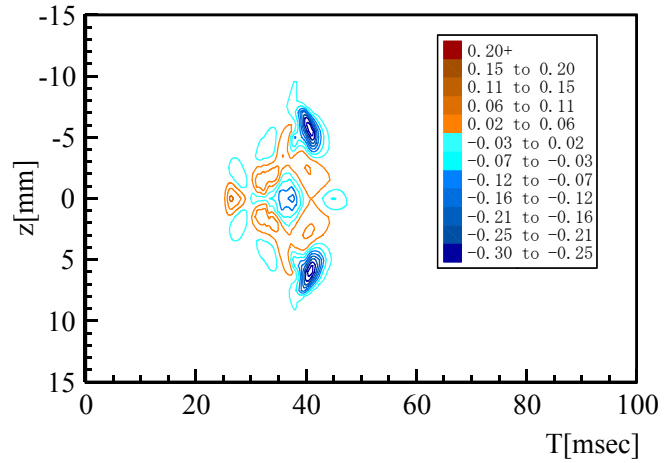


Fig. 10 (b) Plan view of  $\Delta U_{\text{mean}}/U_0$  contour  
for a spot in the transition region.  
 $x=110\text{mm}$ ,  $y=3.4\text{mm}$ .

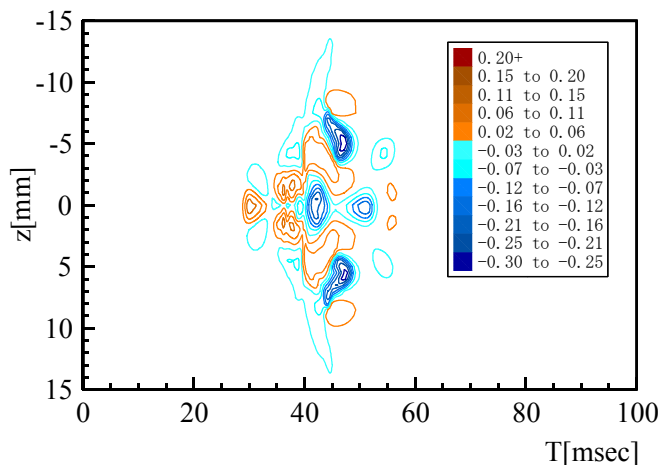


Fig. 10 (c) Plan view of  $\Delta U_{\text{mean}}/U_0$  contour  
for a spot in the transition region.  
 $x=130\text{mm}$ ,  $y=3.4\text{mm}$ .

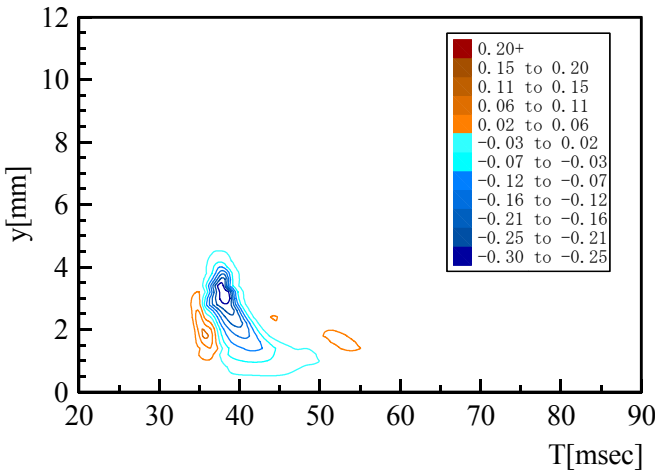


Fig.11 (a) Side view of  $\Delta U_{\text{mean}}/U_0$  contour for the outside low-speed region of a spot at  $x=100\text{mm}$ ,  $z=-5\text{mm}$ .

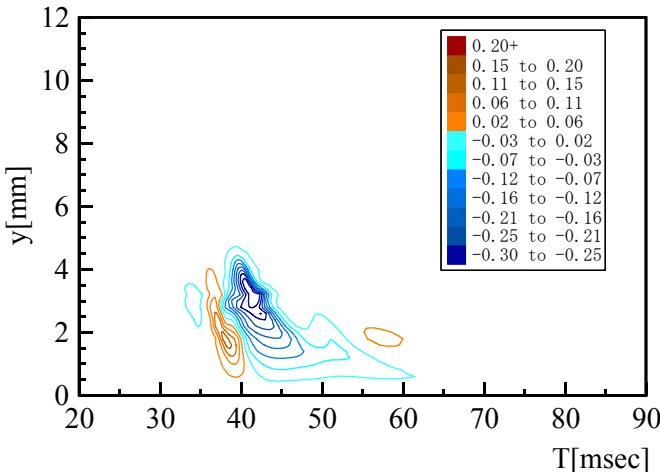


Fig.11 (b) Side view of  $\Delta U_{\text{mean}}/U_0$  contour for the outside low-speed region of a spot at  $x=110\text{mm}$ ,  $z=-5\text{mm}$ .

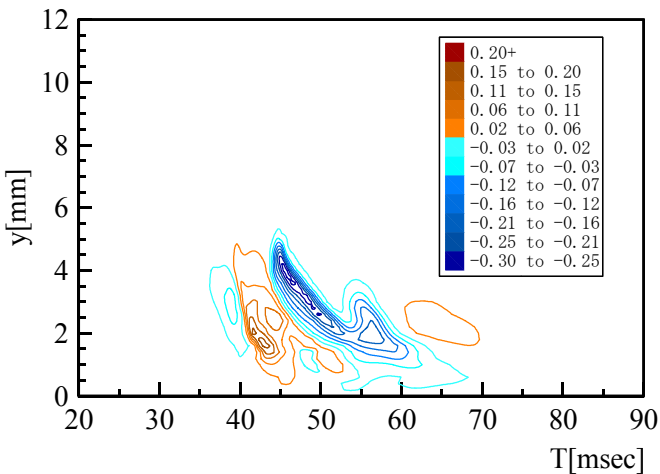


Fig.11 (c) Side view of  $\Delta U_{\text{mean}}/U_0$  contour for the outside low-speed region of a spot at  $x=130\text{mm}$ ,  $z=-5\text{mm}$ .

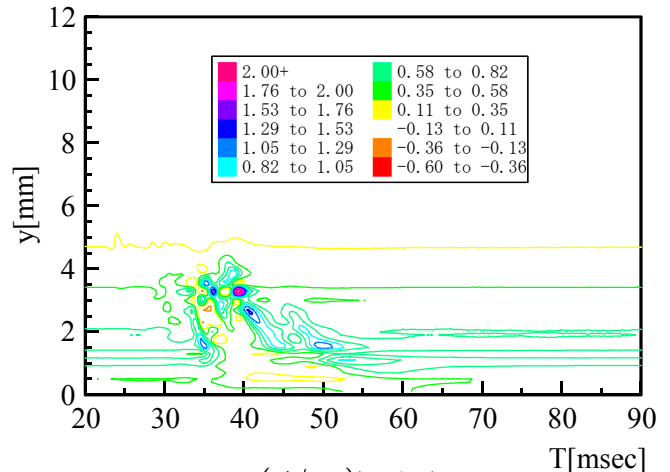


Fig.12 (a)  $(\delta^*/U_0)(\partial U/\partial y)$  contour for the outside low-speed region of a spot at  $x=100\text{mm}$ ,  $z=-5\text{mm}$ .

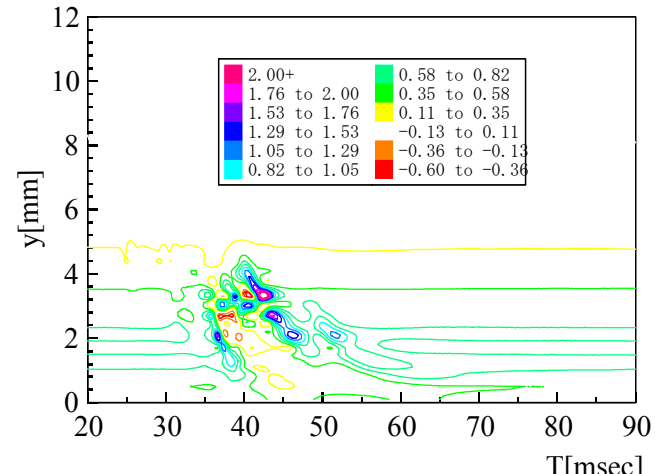


Fig.12 (b)  $(\delta^*/U_0)(\partial U/\partial y)$  contour for the outside low-speed region of a spot at  $x=110\text{mm}$ ,  $z=-5\text{mm}$ .

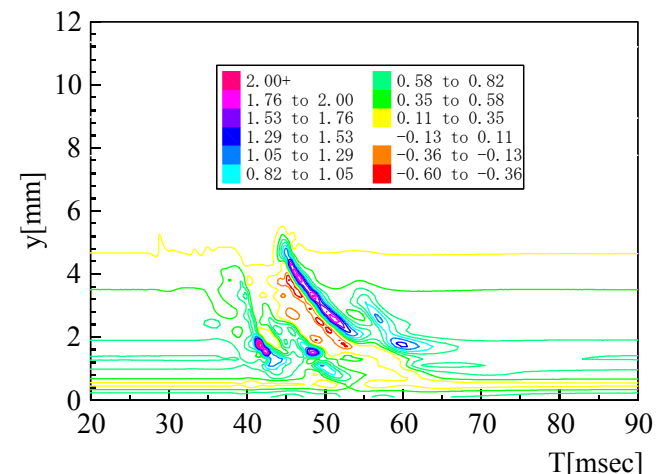


Fig.12 (c)  $(\delta^*/U_0)(\partial U/\partial y)$  contour for the outside low-speed region of a spot at  $x=130\text{mm}$ ,  $z=-5\text{mm}$ .

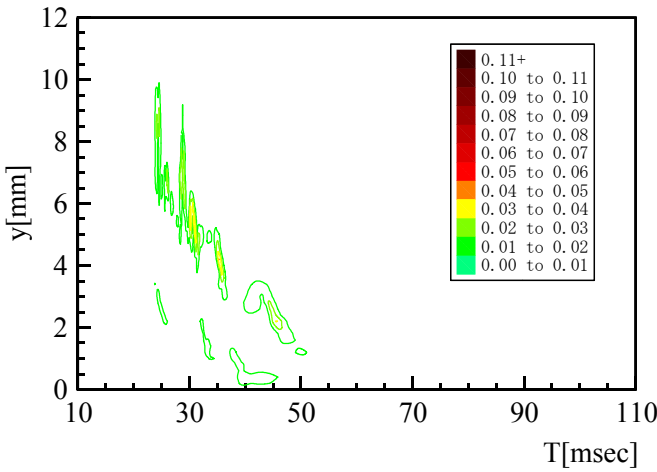


Fig.13 (a) Side view of  $u'/U_0$  contour for a spot at  $x=100\text{mm}$ ,  $z=0$ .

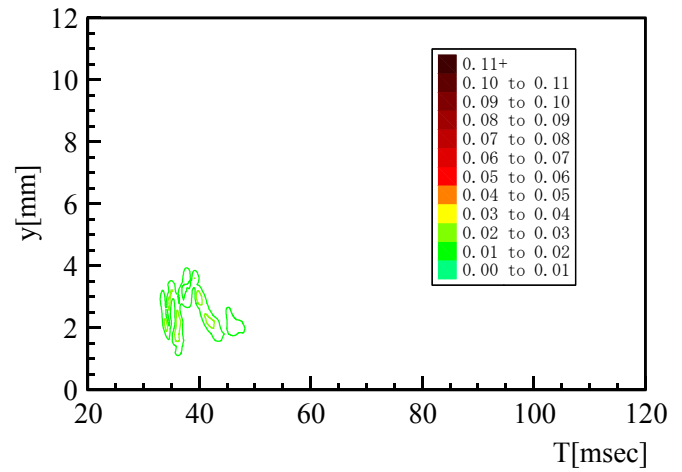


Fig.14 (a) Side view of  $u'/U_0$  contour for a spot at  $x=100\text{mm}$ ,  $z=-5\text{mm}$ .

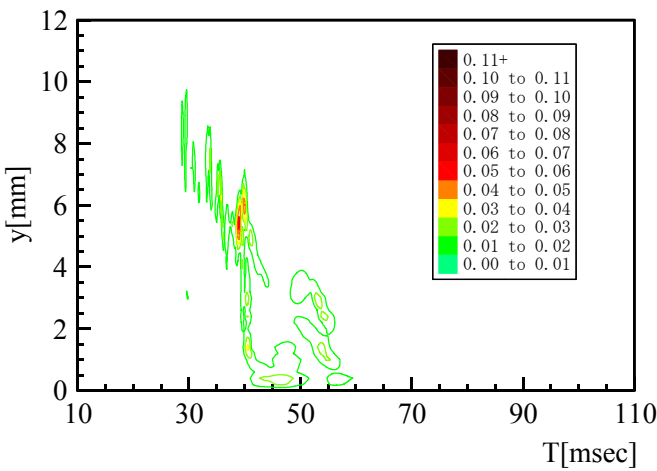


Fig.13 (b) Side view of  $u'/U_0$  contour for a spot at  $x=130\text{mm}$ ,  $z=0$ .

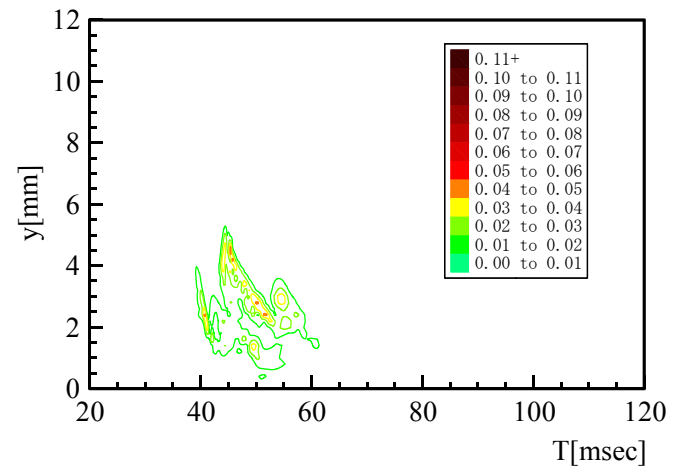


Fig.14 (b) Side view of  $u'/U_0$  contour for a spot at  $x=130\text{mm}$ ,  $z=-5\text{mm}$ .

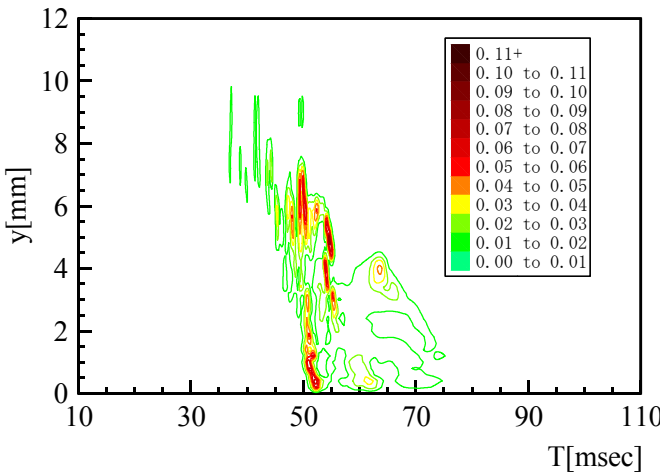


Fig.13 (c) Side view of  $u'/U_0$  contour for a spot at  $x=170\text{mm}$ ,  $z=0$ .

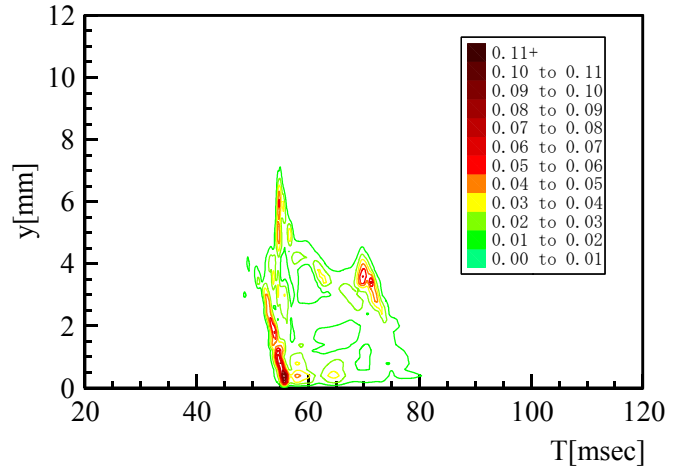


Fig.14 (c) Side view of  $u'/U_0$  contour for a spot at  $x=170\text{mm}$ ,  $z=-6\text{mm}$ .

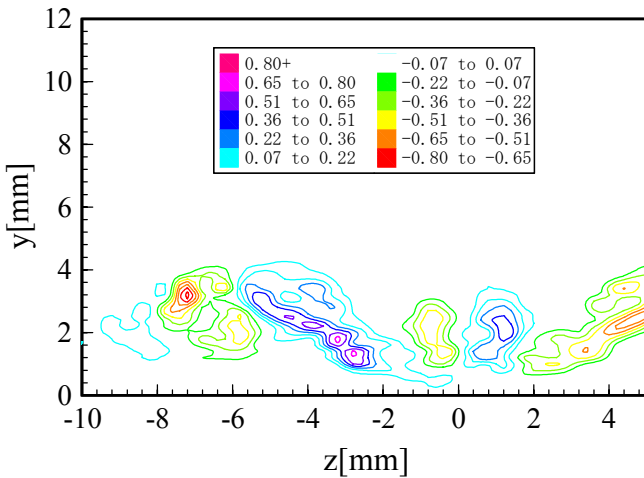


Fig.15 (a) Cross-sectional view of  $(\delta^*/U_0)(\partial U/\partial z)$  contour of a spot at  $x=100$ mm,  $T=37.6$ msec.

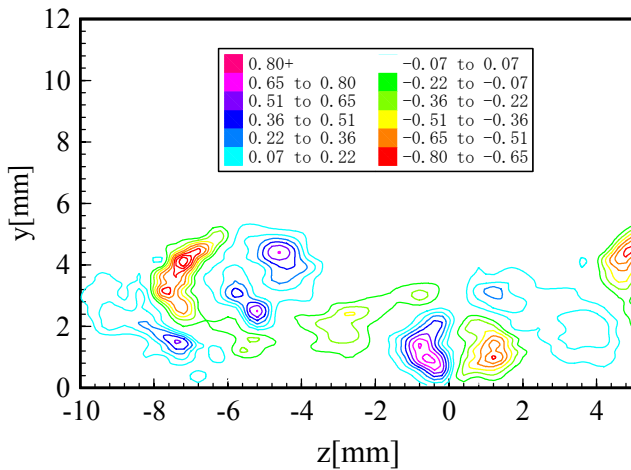


Fig.15 (b) Cross-sectional view of  $(\delta^*/U_0)(\partial U/\partial z)$  contour of a spot at  $x=130$ mm,  $T=44.6$ msec.

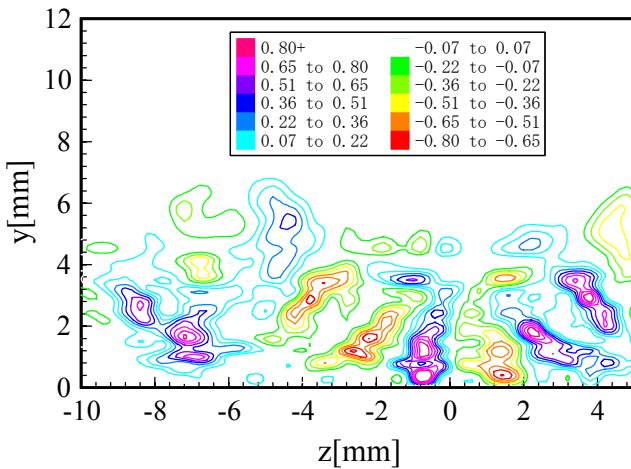


Fig.15 (c) Cross-sectional view of  $(\delta^*/U_0)(\partial U/\partial z)$  contour of a spot at  $x=170$ mm,  $T=55$ msec.

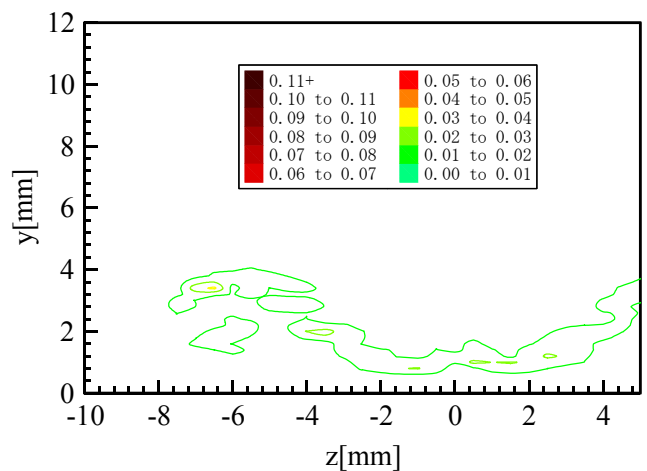


Fig.16 (a) Cross-sectional view of  $u'/U_0$  contour of a spot at  $x=100$ mm,  $T=37.6$ msec.

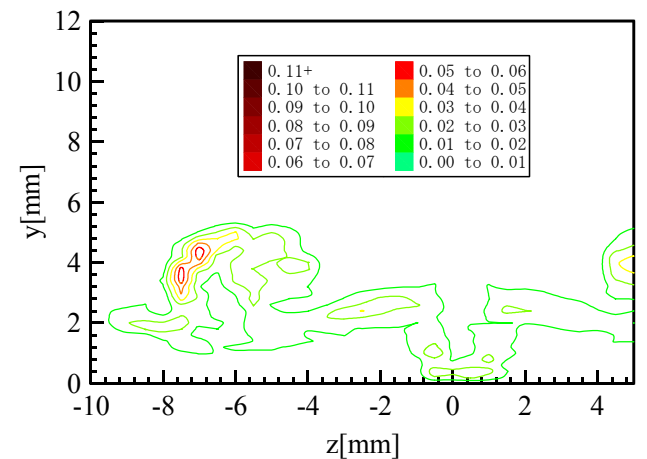


Fig.16 (b) Cross-sectional view of  $u'/U_0$  contour of a spot at  $x=130$ mm,  $T=44.6$ msec.

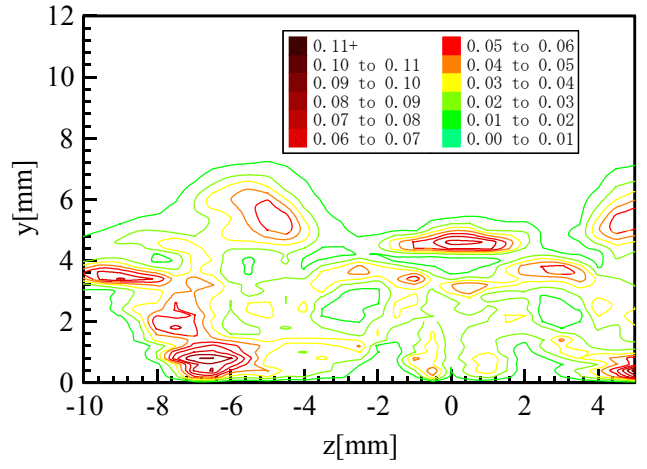


Fig.16 (c) Cross-sectional view of  $u'/U_0$  contour of a spot at  $x=170$ mm,  $T=55$ msec.